Physics of Plasmas

Fuel–shell mix and yield degradation in kinetic shock-driven inertial confinement fusion implosions

Cite as: Phys. Plasmas **29**, 072710 (2022); https://doi.org/10.1063/5.0087905
Submitted: 10 February 2022 • Accepted: 26 June 2022 • Published Online: 20 July 2022

H. Sio, O. Larroche, A. Bose, et al.

Physics of Plasmas ARTICLE scitation.org/journal/php

Fuel–shell mix and yield degradation in kinetic shock-driven inertial confinement fusion implosions

Cite as: Phys. Plasmas **29**, 072710 (2022); doi: 10.1063/5.0087905
Submitted: 10 February 2022 · Accepted: 26 June 2022 ·
Published Online: 20 July 2022

H. Sio,[1,a)] O. Larroche,[2,3] A. Bose,[4] S. Atzeni,[5] J. A. Frenje,[4] N. V. Kabadi,[4] M. Gatu Johnson,[4] C. K. Li,[4] V. Glebov,[6] C. Stoeckl,[6] B. Lahmann,[4] P. J. Adrian,[4] S. P. Regan,[6] A. Birkel,[4] F. H. Seguin,[4] and R. D. Petrasso[4]

AFFILIATIONS

[1]Lawrence Livermore National Laboratory, Livermore, California 94550, USA
[2]CEA DAM DIF, 91297 Arpajon Cedex, France
[3]Université Paris-Saclay, CEA, LMCE, 91680 Bruyères-le-Châtel, France
[4]Plasma Science & Fusion Center, Massachusetts Institute of Technology, Cambridge, Massachusetts 02139, USA
[5]Dipartimento SBAI, Università degli Studi di Roma "La Sapienza," Via Antonio Scarpa 14, 00161 Roma, Italy
[6]Laboratory for Laser Energetics, Rochester, New York 14623, USA

[a)]**Author to whom correspondence should be addressed:** sio1@llnl.gov

ABSTRACT

Fuel–shell mix in kinetic plasma conditions is probed using nuclear and x-ray self-emission in shock-driven, D^3He-gas-filled inertial confinement fusion implosions. As initial gas fill density decreases, measured nuclear yields and ion temperatures are lower than expected as compared to radiation-hydrodynamic simulations. Spatially and temporally resolved x-ray emissions indicate significant mixing at the fuel–shell interface in implosions with low initial gas fill density. This observed fuel–shell mix introduces a substantial amount of shell ions into the center of the implosion prior to and during shock flash and is the key mechanism needed in the kinetic-ion simulations to match experimental nuclear yields.

I. INTRODUCTION

Inertial confinement fusion (ICF) implosions[1] use direct laser drive or indirect x-ray drive to implode a spherical target, compressing the fusion fuel to high density and thermonuclear temperature. The implosion, from ablation to shock propagation to compression to stagnation, transitions through a wide range of densities ($10^{19} - 10^{25}$ cm^{-3}) and temperatures (eV–keV). Radiation-hydrodynamic codes[2–5] play an important role in modeling and understanding these implosions and are orders of magnitude less computationally intensive than fully kinetic codes. Despite hydrodynamic codes' many practical advantages, they are designed to simulate systems that are collisional (with mean free paths much smaller than the length scale of the system). However, certain regions of ICF implosions (ablation, shock propagation, and hohlraum) are often kinetic. Experiments focusing on these kinetic plasma conditions are, therefore, important to establish whether deviations from hydrodynamic expectations exist, and then, whether they are impactful.

The experiments described in this work focus on the shock propagation phase of ICF implosions and on the interactions between fuel and shell ions at the fuel–shell interface, where the high-temperature and low-density plasma conditions lead to a long ion mean free path relative to the implosion radius. Hydrodynamic codes neither do correctly simulate kinetic plasma conditions nor are they expected to. Kinetic models, whether embedded within hydrodynamic codes or implemented in a hybrid fluid-kinetic approach, provide new insights into kinetic mechanisms in these plasmas and an estimate of their relative importance in affecting implosion behaviors. Some consequences of low collisionality in the plasmas include non-Maxwellian features in the particle distribution, loss of energetic tail-ions from the hot spot,[6,7] and ion diffusion. These effects have been studied using kinetic-ion

simulations,[8–11] hydrodynamic codes with reduced-ion-kinetic models,[12] and particle-in-cell simulations.[13,14]

In more collisional implosion conditions,[15] hydrodynamic simulations adequately model measured yields and temperatures, although kinetic simulations can better match time-resolved measurements such as the reaction histories. In contrast, in implosions with lower initial gas fill density, kinetic simulations are needed to capture the overall implosion dynamics. Inclusion of ion diffusion into radiation-hydrodynamic simulations was needed to match the measured reaction profiles[16] and to improve agreements with measured yields[17] and ion temperatures. Nuclear signatures of kinetic mixing have also been studied using separated reactants experiments.[18] In particular, ion diffusion was expected to have played a prominent role in previous experiments[16,19] that measured time-integrated nuclear observables in kinetic ICF implosions. In these previous works, fuel–shell ion mix had significant impacts on the nuclear performance in simulations but had not been observed directly in the experiments. In this work, direct observations of fuel–shell mixing in kinetic plasma conditions using temporally and spatially resolved x-ray self-emission are presented and analyzed with respect to hydrodynamic and kinetic simulations.

The structure of this paper is as follows. Section II outlines the experimental setup and the time-integrated data. Section III describes temporally and spatially resolved x-ray data in the context of fuel–shell mix. Section IV assesses the impact on nuclear performance. Section V summarizes the main result and discusses its implications.

II. OMEGA EXPERIMENTS

The implosion experiments described in this work are conducted at the 60-beam OMEGA laser facility.[20] The targets are thin-glass spherical shell, nominally 2.3 μm thick with an outer diameter of 860 μm. They are filled with either 90%–10% D^3He or 50%–50% D^3He by atomic fraction and, in some cases, trace tritium (for diagnostic purposes). These targets are imploded using all 60 OMEGA laser beams at 351 nm wavelength with a 0.6-ns-square pulse. The laser energy and intensity incident on target are 14.4 kJ and 8×10^{14} W/cm^2, respectively. In these shock-driven implosions, laser ablation drives a strong shock through the shell and into the fuel. During shock flash, this shock rebounds from the center and propagates outward, re-shocking the fuel to fusion temperature and generating fusion products. The laser drive ablates away most of the shell, and there is insufficient shell mass to further compress the implosion, leading to reduced sensitivity to hydrodynamic mix and overall more 1D behaviors.[18]

The plasma conditions during nuclear emission can be varied from hydrodynamic-like to kinetic by changing the initial gas fill density. A data-derived estimate of whether a hydrodynamic description of the system is appropriate is the neutron-averaged Knudsen number $\langle N_K \rangle$, defined here as the neutron-averaged deuteron ion–ion mean free path divided by the minimum fuel radius. The implosions discussed have initial gas fill density between 0.3 and 3.4 mg/cc, corresponding to $\langle N_K \rangle$ between 4 and 0.3 (lower gas fill density corresponds to higher Knudsen number). Because these shock-driven implosions are low convergence (~3–5) and begin to disassemble when the rebounding shock arrives at the fuel–shell interface, they are an ideal system to study implosion dynamics during the shock phase.

In the OMEGA experiments, neutron yields and ion temperatures were measured using neutron time-of-flight detectors.[21] Timing of the neutron production relative to laser drive was measured by the Neutron Temporal Diagnostic.[22,23] The particle x-ray temporal diagnostic[24] and hard x-ray detector[25,26] measured multiple x-ray emission histories using different filtering. X-ray framing cameras[27] recorded temporally and spatially resolved x-ray self-emission images, and two full aperture backscatter systems[28] combined with measured laser energy are used to infer laser absorption.

The experimental neutron yields and neutron-averaged ion temperatures are compared against the 1D radiation-hydrodynamic code LILAC[4] and 1D kinetic-ion Fokker–Planck code FPION.[8] LILAC is a Lagrangian code with flux-limited electron thermal transport (flux limiter = 0.07), and laser absorption is modeled by inverse Bremsstrahlung with refraction. LILAC provides similar results for these shock-driven implosions as two other well-benchmarked hydrodynamic codes (DUED[3] and HYADES[5]). In both the 50%–50% and 90%–10% D^3He implosions with high initial gas fill density (>2 mg/cc), the ratio of experimental to LILAC-simulated DD yield is 0.36. For the low initial gas fill density (<0.8 mg/cc) cases, the ratio of experimental to LILAC-simulated DD yield is 0.06–0.11 [Figs. 1(a) and 1(b)]. This yield trend as implosions transition from a hydrodynamic-like to kinetic plasma regime was first observed by Rosenberg *et al.*,[19] and the inclusion of an ion diffusion model (and other reduced-kinetic models) in a radiation-hydrodynamic code was able to better capture the yield trend.[12] Experimentally, we also observed that the neutron-averaged DD temperatures are lower than simulated, and this discrepancy increases as implosions become more kinetic [Figs. 1(c) and 1(d)]. Each data point in Fig. 1 is averaged over three shots (for the 50%–50% D^3He implosions) or averaged over five shots (for the 90%–10% D^3He implosions). The error bars represent the scatter in the experiment between nominally identical implosions.

FPION-simulated yield and ion temperatures are also plotted in Fig. 1. FPION[8] is a Vlasov–Fokker–Planck ion-kinetic code. The fuel ions are treated as kinetic, while the electrons are treated as a fluid. A hybrid kinetic-fluid approach is used to simulate these implosions, using initial and boundary conditions from radiation-hydrodynamic (in this case, HYADES[5]) simulations.

The time when kinetic calculation begins is chosen sufficiently late, such that we do not need to simulate too much cold and dense matter with the kinetic code, and sufficiently early to not miss too much of the kinetic behaviors in the implosion center. Similarly, the boundary condition for the kinetic simulation is chosen sufficiently far out into the pusher to correctly treat the mixing between fuel and shell ions, but not too far out as to include regions of the pusher that will be ablated by the laser. This boundary condition is Lagrangian and follows a cell of the hydrosimulation rather than at a fixed position in space. The initial conditions for the FPION simulations (density, temperature, velocity, and charge state) are shown in Fig. 8 in the Appendix.

The strong scaling of Coulomb collision times with the mass and charge of the particles results in vastly different relaxation timescales when considering the collisional interaction of the SiO_2 shell with the

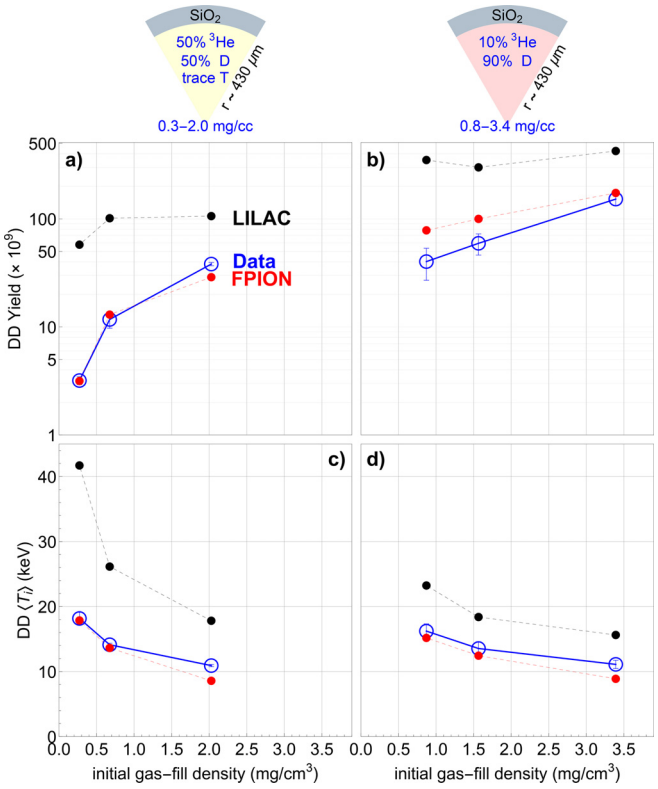

FIG. 1. As a function of initial gas-fill density, (a) and (c) show the DD-n yield and neutron-averaged DD ion temperature for implosions with 50%–50% D^3He gas fill, respectively. (b) and (d) The DD-n yield and neutron-averaged DD ion temperature for implosions with 90%–10% D^3He gas fill, respectively. Yields and ion temperatures simulated by the hydrodynamic code LILAC and kinetic-ion code FPION are shown in black and red, respectively. These data are also presented in tabular form in Table I.

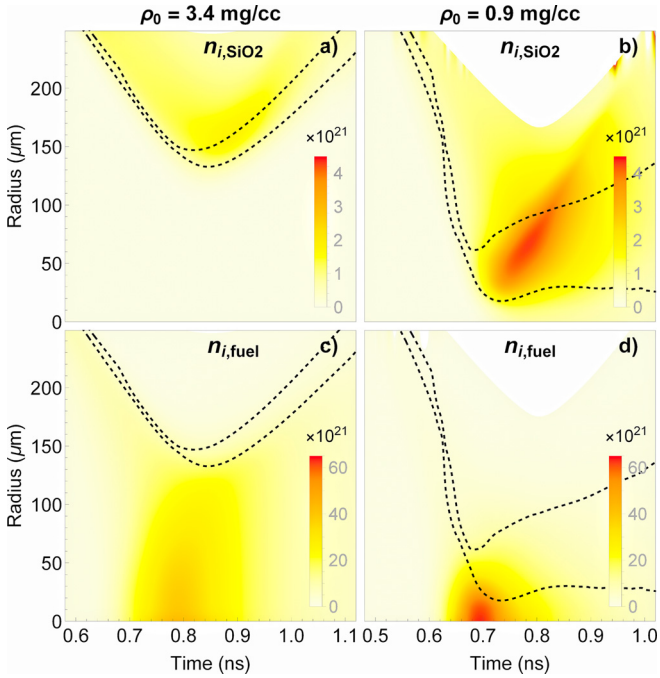

FIG. 2. FPION-simulated fuel and shell ion densities for two 90%–10% D^3He implosions with different initial gas fill densities. (a) and (c) The shell and fuel ion densities, respectively, for a D^3He implosion with an initial gas fill density of 3.4 mg/cc (shot 82 745). (b) and (d) The shell and fuel ion densities, respectively, for a D^3He implosion with an initial gas-fill density of 0.9 mg/cc (shot 82 740). The black-dashed lines indicate the approximate region of fuel–shell ion mix in the kinetic simulation.

D^3He gas. The SiO_2 included in the kinetic simulation domain (with much shorter collision timescales relative to D^3He and, thus, expected to remain close to local thermodynamic equilibrium) is treated as a single-fluid species. The primary reason for treating the SiO_2 as a single-fluid species is the very small ion mean free path between the Si and O ions in the pusher region in most of the space-time domain of the simulation (comparable to the SiO_2 mean free path shown in Fig. 3). In addition, the pusher ions are accelerated from the electric field arising from the electron pressure gradient, and as such, the ion velocity is related to the ion charge-to-mass ratio Z/A. Both the Si and O ions are expected to be fully ionized with the same Z/A, with $Z/A = 14/28$ for Si and $Z/A = 8/16$ for O, leading to the same acceleration. Finally, the thermal velocity of the pusher ions is much smaller than the bulk-fluid velocity, so no significant ion diffusion between Si and O is expected. More details on collision treatments are described in reference.[29]

The FPION-simulated yields are within a factor of two of the measured values, and the agreement is better with the 50%–50% D^3He implosions as compared to the 90%–10% D^3He implosions. Radiation transport is expected to impact neither hydrodynamics nor nuclear performance in these systems, and this is confirmed by running simulations without radiation transport vs with a gray radiation diffusion model. Overall, FPION is able to much better match the yield and temperature trends as compared to LILAC especially as initial gas fill density decreases.

In addition, FPION simulations show the development of a fast-ion population in the shock structure. Such features in the particle distribution are far from thermal equilibrium and cannot be accounted for using perturbation-based transport models. The fast ion population in the particle distribution and the loss of these fast ions most relevant for fusion reactions are important to model properly but, by themselves[30] and without fuel–shell ion diffusion, cannot reproduce the measured yields.

Figure 2 shows radius-time plots, showing the FPION-simulated fuel and shell ion densities for two 90%–10% D^3He implosions: one with high initial gas fill density (3.4 mg/cc) and another with low initial gas fill density (0.9 mg/cc). The shell plasma conditions for these two cases are initially similar to they share the same laser drive. Figures 2(a) and 2(c) show that when the initial gas fill density is high, there is a clear boundary between the fuel and shell ions before and after peak compression because of higher collisionality at the fuel–shell interface. However, in Figs. 2(b) and 2(d), the region of fuel–shell ion interpenetration is much wider. For illustrative purpose, the mix boundaries (black-dashed lines) are

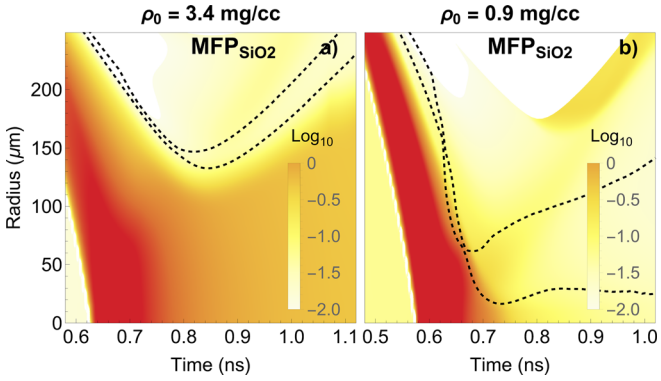

FIG. 3. FPION-simulated mean free path (μm) of a thermal SiO_2 ion for two 90%–10% D^3He implosions with different initial gas fill densities at (a) 3.4 mg/cc (shot 82 745) and (b) 0.9 mg/cc (shot 82 740). The black-dashed lines indicate the approximate region of fuel–shell ion mix in the kinetic simulation.

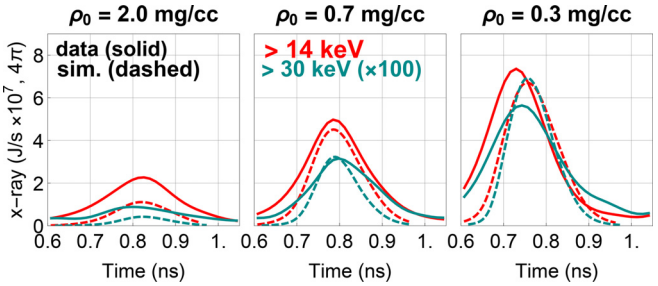

FIG. 4. PXTD-measured (solid) and FPION-simulated (dashed) x-ray emission histories above 14 keV (red) and above 30 keV (teal) for 50%–50% D^3He implosions. The above 30 keV (teal) signal is scaled by a factor of 100 to display on the same scale. The initial gas fill densities are 2.0 mg/cc (shot 82 615), 0.7 mg/cc (shot 82 617), and 0.3 mg/cc (shot 82 620) (left, center, and right, respectively).

defined by where the inward-diffusing SiO_2-ion density falls to 50% of its peak value and by where the outward-diffusing fuel–ion density falls to 20% of its peak value.

The difference in the mean free path of a thermal SiO_2 ion in the region of fuel–shell ion mix (between dashed lines) for implosions with different initial gas fill densities is illustrated in Fig. 3, supporting the intuition of enhanced diffusion at the fuel–shell interface with lower initial gas fill density. The slowing down distance of a shell ion will be even longer than its thermal mean free path because the implosion velocity is higher than the thermal velocity. After peak compression, the mean free path in the kinetic simulation is actually shorter in the low-gas-fill-density implosion center because of SiO_2 presence in the fuel region.

The key topological change in the kinetic simulations as implosions transition from hydrodynamic-like to kinetic plasma conditions is significantly increased ion diffusion across the fuel–shell interface. The fuel ions diffuse into the shell plasma, lowering density at the implosion center. The shell ions diffuse into the central fuel region, increasing x-ray emission. This strong fuel–shell mixing occurs before the rebounding shock arrives at the fuel–shell interface and is distinct from hydrodynamic instabilities.

III. X-RAY MEASUREMENTS OF FUEL–SHELL MIX

This section will address the physics mechanisms driving the time-averaged measurements in Sec. II, focusing on x-ray measurements that have not been discussed in previous works. The extent of the diffusive mixing between the fuel and shell ions developed in the kinetic simulations is not a small perturbation and, as such, should be observable in spatially and temporally resolved x-ray self-emissions.

Measured x-ray emission histories in these shock-driven implosions support enhanced SiO_2 mixing into the implosion center. X-ray emission histories above 14 keV and above 30 keV are measured using the particle x-ray temporal diagnostic (PXTD).[24] X-ray emissions incident on different scintillator channels generate scintillator photons that are optically relayed to a streak camera. The absolute x-ray emissions are obtained by cross calibrating to the hard x-ray detector (HXRD).[26]

Figure 4 shows the measured x-ray histories for three different initial gas fill densities: 2.0, 0.7, and 0.3 mg/cc. Both the absolute signal magnitudes and relative trends are reasonably captured in the synthetic x-ray histories generated from FPION post-shot simulations. Absolute x-ray emission increase was also observed in other x-ray diagnostics sensitive to x rays between 1 and 10 keV. In comparison, while synthetic x-ray emissions from hydrodynamic simulations also show an increasing trend with lower gas fill density, the absolute x-ray emission level is much higher than measured.

Similarly, sharp differences in x-ray framing camera images between implosions with high and low initial gas fill density strongly support the enhanced fuel–shell mixing interpretation. Simulated SiO_2 emission spectrum at ablation plasma temperature (~1–2 keV) has strong emission lines between 2 and 2.5 keV. The x-ray framing camera is filtered with 125 μm of beryllium to filter out x-ray emission below 1.5 keV. Because of the strong dependence on Bremsstrahlung emission on Z and the high ratio of shell mass to fuel mass, x-ray emission is dominated by SiO_2 emission. Each image is integrated over 30–40 ps[27] and intensity-corrected using a series of optical density steps with known exposures. Synthetic x-ray images are post-processed from FPION x-ray emission profiles, accounting for the framing camera integration time, finite pinhole size, motional blurring, x-ray transmission through filter, and x-ray energy deposition in the film.[31,32]

In the implosion with high initial gas fill density (3.4 mg/cc), recorded x-ray images from shock convergence through peak emission show well-defined emission from the shell plasma (Fig. 5, left), and corresponding synthetic FPION images demonstrate very good agreement in both profile shape and emission size. For the implosion with low initial gas fill density (0.9 mg/cc), the recorded x-ray images show markedly different behaviors, with blurred shell emission early in time, and later on, indistinguishable emission between shell and fuel plasmas (Fig. 5, right). The measured x-ray images as a function of time are indicative of the enhanced diffusive mixing observed in kinetic simulations between the fuel and shell ions. In addition, synthetic FPION x-ray images are able to reproduce the emission profile

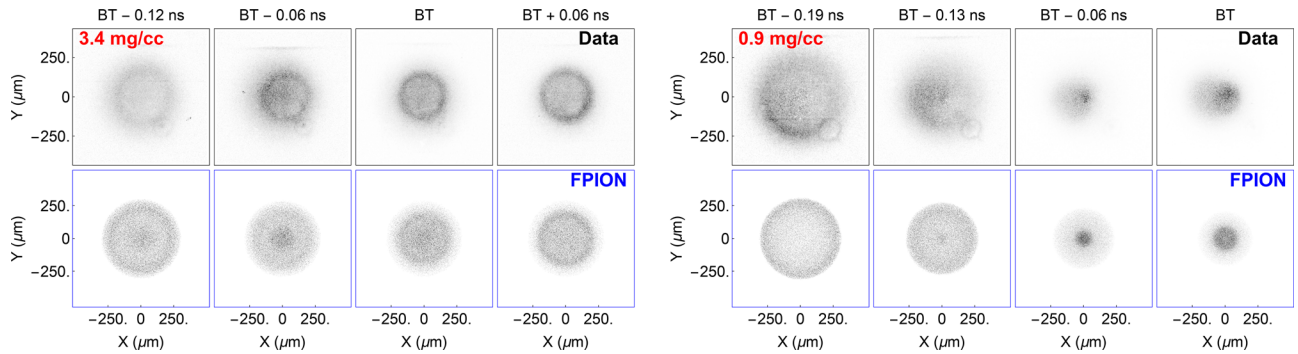

FIG. 5. On the left, measured (top-left row) and FPION-simulated (bottom-left row) x-ray images for a 90%–10% D^3He implosion with an initial gas-fill density of 3.4 mg/cc (shot 82 745). Time progresses from left to right relative to the time of peak x-ray emission (bang time or BT). On the right, measured (top-right row) and FPION-simulated (bottom-right row) x-ray images for a 90%–10% D^3He implosion with an initial gas-fill density of 0.9 mg/cc (shot 82 740).

changes observed in the experiment. In the kinetic case, the synthetic x-ray images clearly demonstrate how increased ion diffusion across the fuel–shell interface translates into broadened shell emission profiles observed in the experiment.

IV. IMPACT ON NUCLEAR PERFORMANCE

To discuss the impact of observed fuel–shell mixing on nuclear performance in these kinetic implosions, it is helpful to consider the impact of other kinetic mechanisms (fast-ion tail and other non-Maxwellian features). Figure 6 shows the FPION-simulated DD and D^3He reaction histories for two implosions with initial gas-fill density of 3.4 and 0.9 mg/cc, respectively. These reaction histories are calculated from the same simulation outputs using two different approaches. The dashed lines are reaction histories calculated directly from the ion distribution function. The solid lines are reaction histories calculated from Maxwellian quantities (density and temperature). While there are non-Maxwellian features in the ion distribution function, the calculated differences in the nuclear reaction rate are at most 25%.

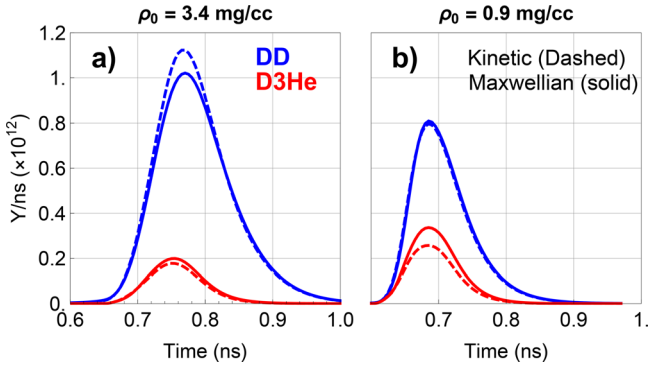

FIG. 6. FPION-simulated DD (blue) and D^3He (red) nuclear reaction histories for (a) 90%–10% D^3He implosion with an initial gas-fill density of 3.4 mg/cc (shot 82 745) and (b) an initial gas-fill density of 0.9 mg/cc (shot 82 740). Reaction histories are calculated directly from the distribution function (dashed) and also from Maxwellian quantities (solid).

In contrast, kinetic simulations showed a much stronger impact on nuclear yield due to fuel–shell mixing. Kinetic simulations of low-gas-fill-density shock-driven implosions without ion diffusion across the fuel–shell interface have ∼8× higher nuclear yield as compared to the experiment.[30] It is only with the inclusion of ion diffusion that kinetic simulations can reach good agreement with the experiment.[29] The simulation conclusion that strong pusher-fuel mixing is needed to correctly interpret low-density shock-driven implosions is now validated by experimental x-ray observation of strong fuel–shell mix.

X-ray emission histories, in combination with time sequences of spatially resolved x-ray images, provided compelling experimental evidence that support enhanced ion diffusion across the fuel–shell interface prior to shock flash in these kinetic implosions. The inward diffusion of the SiO_2 ions increases radiative loss and absolute x-ray emission, while the outward diffusion of the fuel ions reduces fuel–ion density and nuclear yields in the implosion center. In the kinetic simulations inside the mix region, the ion and electron temperatures are only weakly coupled (ion-electron thermal equilibration time ∼1 ns). In contrast, the thermal equilibration time between the SiO_2 and D^3He ions is only ∼80 ps. This is smaller than the neutron production width of ∼130 ps and suggests that both outward diffusion of the fuel ions (reducing density) and energy transfer to the shell ions (lowering temperature) impact the nuclear yield.

To illustrate these effects, Fig. 7 shows the FPION-simulated fuel and shell ion density profiles, focusing on two particular times in the implosion. Figures 7(a) and 7(b) are the density profiles when the inward propagating shock is about to converge at the center. At this time, most of the shell has already been ablated away, and already significant interpenetration of fuel and shell ions can be seen in the implosion with lower initial gas fill density. Figures 7(c) and 7(d) are the density profiles near the time of peak emission, and in the lower density case, the diffusive mixing has increased in time. In contrast, the implosion with the higher initial gas fill density maintained a more clear separation between fuel and shell ions despite similar coronal plasma conditions. While the fuel–ion temperature profile for the 3.4 mg/cc implosion [Fig. 7(c), red] is centrally peaked, the fuel–ion temperature profile for the 0.9 mg/cc implosion [Fig. 7(d), red] is lower in the central region where significant SiO_2 ions are present.

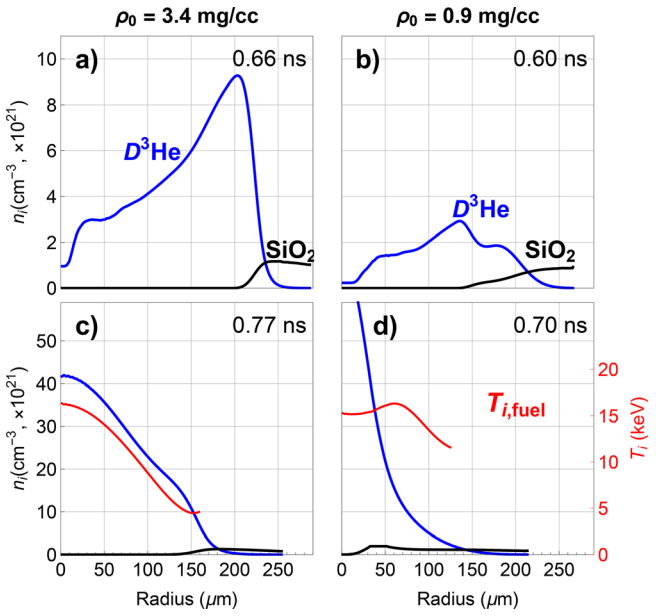

FIG. 7. FPION-simulated fuel (blue) and shell (black) ion density profiles for a 90%–10% D^3He implosions with initial gas fill density at 3.4 mg/cc (left column, shot 82 745) and at 0.9 mg/cc (right column, shot 82 740). The profiles in (a) and (b) are at the time when the strong shock reaches the center of the implosion. The profiles in (c) and (d) are near peak emission. In (c) and (d), the deuteron ion temperature profile is shown in red.

V. CONCLUSION

Substantial mix across the fuel–shell interface in kinetic implosion conditions is directly observed using temporally and spatially resolved x-ray emission, and this enhanced mixing at the interface, in turn, affects implosion performance by reducing hot spot fuel–ion density and lowering fuel–ion temperature. This mix mechanism is distinct from hydrodynamic Rayleigh–Taylor mix during the compression phase and begins to develop during shock propagation.

The strong diffusive mixing and non-Maxwellian features in these kinetic simulations go beyond small perturbations from thermal equilibrium and require a fully kinetic treatment. This raises the question of whether a hydrodynamic treatment, even with transport models based on perturbations from thermal equilibrium, is sufficient during different times in an ignition-relevant implosion, for example, at shock breakout at the DT-ice/DT-vapor interface,[33] during shock propagation,[10,11] and inside the hohlraum.[34–36] To understand and accurately simulate these similarly kinetic ICF plasma conditions, improved physics models should be developed to complement existing hydrodynamic simulation capabilities.

ACKNOWLEDGMENTS

The authors thank R. Frankel and E. Doeg for contributing to the fielding and processing of CR-39 data used in this work as well as the OMEGA operations crew for their help in executing these experiments. The targets and gas-fills are coordinated by General Atomics (GA) and the Lawrence Livermore National Laboratory (LLNL) and Laboratory for Laser Energetics (LLE) tritium facilities. This work was performed under the auspices of the U.S. Department of Energy by Lawrence Livermore National Laboratory under Contract No. DE-AC52–07NA27344 and based upon work supported by the Department of Energy, National Nuclear Security Administration under Award Nos. DE-NA0001857, DE-NA0002949, DE-NA0002905, and DE-NA0003868. This work was also supported in part by National Laser Users' Facility (NLUF) (No. DE-NA0002035). H.S. was supported by a U.S. Department of Energy National Nuclear Security Administration Stewardship Science Graduate Fellowship (NNSA SSGF) fellowship (No. DE-FC52–08NA28752) during part of this work. The work of S.A. has been carried out within the framework of the EUROfusion Consortium, funded by the European Union via the Euratom Research and Training Programme (Grant Agreement No. 101052200—EUROfusion, Enabling Research Project No. ENR-IFE.01.CEA).

AUTHOR DECLARATIONS

Conflict of Interest

The authors have no conflicts to disclose.

Author Contributions

Hong Sio: Conceptualization (lead); Data curation (lead); Formal analysis (lead); Investigation (lead); Methodology (equal); Writing – original draft (lead); Writing – review and editing (lead). **Christian Stoeckl:** Data curation (supporting). **Brandon Lahmann:** Data curation (supporting); Methodology (supporting). **Patrick Adrian:** Data curation (supporting). **Sean Patrick Regan:** Resources (supporting). **Andrew Birkel:** Data curation (supporting). **Fredrick H. Seguin:** Data curation (supporting); Methodology (supporting). **Richard Petrasso:** Conceptualization (lead); Funding acquisition (lead); Investigation (equal); Project administration (equal); Resources (equal); Supervision (lead); Writing – review and editing (equal). **Olivier Larroche:** Formal analysis (equal); Methodology (equal); Writing – review and editing (supporting). **Arijit Bose:** Formal analysis (supporting); Methodology (supporting); Writing – review and editing (supporting). **Stefano Atzeni:** Formal analysis (supporting); Writing – review and editing (supporting). **Johan A. Frenje:** Conceptualization (equal); Funding acquisition (lead); Project administration (equal); Resources (equal); Supervision (equal); Writing – review and editing (supporting). **Neel V. Kabadi:** Data curation (supporting); Methodology (supporting); Writing – review and editing (supporting). **Maria Gatu Johnson:** Investigation (supporting); Supervision (supporting). **Chikang Li:** Conceptualization (supporting); Funding acquisition (supporting); Investigation (supporting); Supervision (supporting). **Vladimir Yu. Glebov:** Data curation (supporting).

DATA AVAILABILITY

The data that support the findings of this study are available from the corresponding author upon reasonable request.

APPENDIX: DATA TABLE AND SIMULATION INITIAL CONDITIONS

Figure 8 shows initial conditions from 1D hydrodynamic HYADES simulations for FPION. Table I shows yields and ion temperatures (T_i) as measured in the experiments and as simulated by LILAC and FPION.

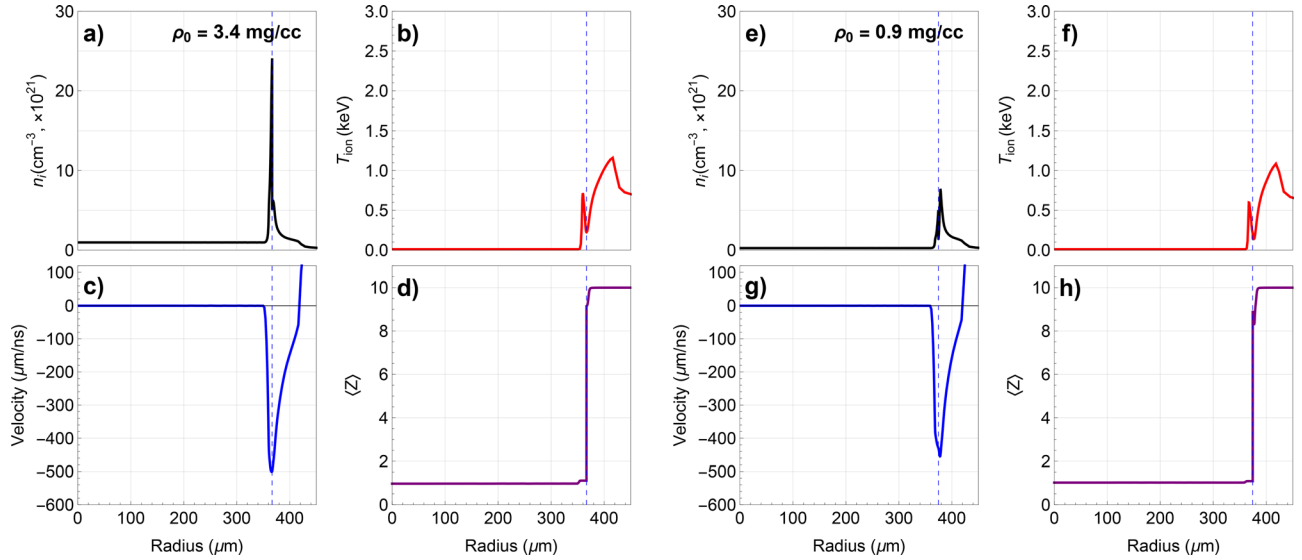

FIG. 8. Initial conditions from 1D hydrodynamic HYADES simulations for FPION. (a)–(d) The initial ion density, ion temperature, fluid velocity, and charge state, respectively, as a function of radius for an implosion with an initial gas-fill density of 3.4 mg/cc (82 745), at t = 0.42 ns. (e)–(h) The initial ion density, ion temperature, fluid velocity, and charge state, respectively, as a function of radius for an implosion with initial gas-fill density of 0.9 mg/cc (82 740) at t = 0.37 ns. The blue-dashed line is the fuel–shell interface in the hydrodynamic simulations.

TABLE I. Yields and ion temperatures (T_i) as measured in the experiments and as simulated by LILAC and FPION. The nominal outer diameter of these targets is 860 μm, with a 2.3-μm-thick SiO_2 shell. Data in each row are averaged over three shots (for the 50%–50% D^3He implosions) or averaged over five shots (for the 90%–10% D^3He implosions), and the uncertainties represent scatter in the data. ρ_0, f_D, and f_{3He} refer to the initial gas fill density, deuterium fraction in the gas fill, and helium-3 fraction in the gas fill, respectively.

				Experiment				LILAC				FPION			
				DD		D^3He		DD		D^3He		DD		D^3He	
	ρ_0 mg/cc	f_D	f_{He3}	Yield ×10^{10}	T_i keV	Yield ×10^{10}	T_i keV	Yield ×10^{10}	T_i keV	Yield ×10^{10}	T_i keV	Yield ×10^{10}	T_i keV	Yield ×10^{10}	T_i keV
$f_D = 0.5$	2.0	0.50	0.50	3.8 ± 0.1	10.9 ± 0.2	4.6 ± 0.8	13.6 ± 1.8	10.6	17.8	28.4	27.7	2.9	8.6	3.2	13.3
	0.7	0.51	0.49	1.2 ± 0.2	14.1 ± 0.2	3.3 ± 0.6	17.7 ± 1.7	10.1	26.1	46.4	29.6	1.3	13.6	3.0	16.9
	0.3	0.48	0.49	0.3 ± 0.03	18.2 ± 0.9	1.4 ± 0.4	25.8 ± 3.2	5.8	41.7	53.5	44.9	0.3	17.9	1.5	23.4
$f_D = 0.9$	3.4	0.89	0.11	15.2 ± 2.0	11.1 ± 0.6	2.0 ± 0.3	11.0 ± 0.7	42.5	15.6	10.3	25.8	17.4	8.9	1.8	12.2
	1.6	0.90	0.10	5.9 ± 1.3	13.5 ± 1.1	1.8 ± 0.2	13.5 ± 0.9	30.0	18.4	8.2	25.9	10.0	12.4	2.0	16.0
	0.9	0.91	0.09	4.0 ± 1.3	16.2 ± x1.1	1.7 ± 0.5	16.3 ± 1.4	35.0	23.2	13.7	27.5	7.8	15.2	2.3	18.9

REFERENCES

[1]J. Lindl, "Development of the indirect-drive approach to inertial confinement fusion and the target physics basis for ignition and gain," Phys. Plasmas **2**, 3933 (1995).

[2]M. M. Marinak, G. D. Kerbel, N. A. Gentile, O. Jones, D. Munro, S. Pollaine, T. R. Dittrich, and S. W. Haan, "Three-dimensional HYDRA simulations of National Ignition Facility targets," Phys. Plasmas **8**, 2275–2280 (2001).

[3]S. Atzeni, A. Schiavi, F. Califano, F. Cattani, F. Cornolti, D. D. Sarto, T. Liseykina, A. Macchi, and F. Pegoraro, "Fluid and kinetic simulation of inertial confinement fusion plasmas," Comput. Phys. Commun. **169**, 153–159 (2005).

[4]J. Delettrez, "Thermal electron transport in direct-drive laser fusion," Can. J. Phys. **64**, 932–943 (1986).

[5]J. T. Larsen and S. M. Lane, "HYADES—A plasma hydrodynamics code for dense plasma studies," J. Quant. Spectrosc. Radiat. Transfer **51**, 179–186 (1994).

[6]K. Molvig, N. M. Hoffman, B. J. Albright, E. M. Nelson, and R. B. Webster, "Knudsen layer reduction of fusion reactivity," Phys. Rev. Lett. **109**, 095001 (2012).

[7]B. J. Albright, K. Molvig, C.-K. Huang, A. N. Simakov, E. S. Dodd, N. M. Hoffman, G. Kagan, and P. F. Schmit, "Revised Knudsen-layer reduction of fusion reactivity," Phys. Plasmas **20**, 122705 (2013).

[8]O. Larroche, "Kinetic simulations of fuel ion transport in ICF target implosions," Eur. Phys. J. D **27**, 131–146 (2003).

[9]B. D. Keenan, A. N. Simakov, L. Chacón, and W. T. Taitano, "Deciphering the kinetic structure of multi-ion plasma shocks," Phys. Rev. E **96**, 053203 (2017).

[10]B. D. Keenan, A. N. Simakov, W. T. Taitano, and L. Chacón, "Ion species stratification within strong shocks in two-ion plasmas," Phys. Plasmas **25**, 032103 (2018).

[11]W. T. Taitano, A. N. Simakov, L. Chacón, and B. Keenan, "Yield degradation in inertial-confinement-fusion implosions due to shock-driven kinetic fuel-species stratification and viscous heating," Phys. Plasmas **25**, 056310 (2018).

[12]N. M. Hoffman, G. B. Zimmerman, K. Molvig, H. G. Rinderknecht, M. J. Rosenberg, A. N. Simakov, H. Sio, A. B. Zylstra, M. G. Johnson, F. H. Séguin, A. Johan, C. K. Li, R. D. Petrasso, D. M. Higdon, G. Srinivasan, V. Y. Glebov, W. Seka, T. C. Sangster, N. M. Hoffman, G. B. Zimmerman, K. Molvig, and H. G. Rinderknecht, "Approximate models for the ion-kinetic regime in inertial-confinement-fusion capsule implosions," Phys. Plasmas **22**, 052707 (2015).
[13]A. Le, T. J. T. Kwan, M. J. Schmitt, H. W. Herrmann, and S. H. Batha, "Simulation and assessment of ion kinetic effects in a direct-drive capsule implosion experiment," Phys. Plasmas **23**, 102705 (2016).
[14]C. Bellei and P. A. Amendt, "Shock-induced mix across an ideal interface," Phys. Plasmas **24**, 040703 (2017).
[15]H. Sio, O. Larroche, S. Atzeni, N. V. Kabadi, J. A. Frenje, M. G. Johnson, C. Stoeckl, C. K. Li, C. J. Forrest, V. Glebov, P. J. Adrian, A. Bose, A. Birkel, S. P. Regan, F. H. Seguin, and R. D. Petrasso, "Probing ion species separation and ion thermal decoupling in shock-driven implosions using multiple nuclear reaction histories," Phys. Plasmas **26**, 072703 (2019).
[16]M. J. Rosenberg, F. H. Séguin, P. A. Amendt, S. Atzeni, H. G. Rinderknecht, N. M. Hoffman, A. B. Zylstra, C. K. Li, H. Sio, M. G. Johnson, J. A. Frenje, R. D. Petrasso, V. Y. Glebov, C. Stoeckl, W. Seka, F. J. Marshall, J. A. Delettrez, T. C. Sangster, R. Betti, S. C. Wilks, J. Pino, G. Kagan, K. Molvig, and A. Nikroo, "Assessment of ion kinetic effects in shock-driven inertial confinement fusion implosions using fusion burn imaging," Phys. Plasmas **22**, 062702 (2015).
[17]Y. Kim, H. W. Herrmann, N. M. Hoffman, M. J. Schmitt, G. Kagan, A. M. McEvoy, A. B. Zylstra, J. M. Smidt, S. Gales, A. Leatherland, M. Rubery, M. G. Johnson, J. A. Frenje, V. Y. Glebov, and C. Forrest, "First observation of increased DT yield over prediction due to addition of hydrogen," Phys. Plasmas **28**, 012707 (2021).
[18]H. G. Rinderknecht, H. Sio, C. K. Li, a B. Zylstra, M. J. Rosenberg, P. Amendt, J. Delettrez, C. Bellei, J. A. Frenje, M. G. Johnson, F. H. Séguin, R. D. Petrasso, R. Betti, V. Y. Glebov, D. D. Meyerhofer, T. C. Sangster, C. Stoeckl, O. Landen, V. A. Smalyuk, S. Wilks, A. Greenwood, and A. Nikroo, "First observations of nonhydrodynamic mix at the fuel-shell interface in shock-driven inertial confinement implosions," Phys. Rev. Lett. **112**, 135001 (2014).
[19]M. J. Rosenberg, H. G. Rinderknecht, N. M. Hoffman, P. A. Amendt, S. Atzeni, A. B. Zylstra, C. K. Li, F. H. Séguin, H. Sio, M. G. Johnson, J. A. Frenje, R. D. Petrasso, V. Y. Glebov, C. Stoeckl, W. Seka, F. J. Marshall, J. A. Delettrez, T. C. Sangster, R. Betti, V. N. Goncharov, D. D. Meyerhofer, S. Skupsky, C. Bellei, J. Pino, S. C. Wilks, G. Kagan, K. Molvig, and A. Nikroo, "Exploration of the transition from the hydrodynamiclike to the strongly kinetic regime in shock-driven implosions," Phys. Rev. Lett. **112**, 185001 (2014).
[20]T. Boehly, D. Brown, R. Craxton, R. Keck, J. Knauer, J. Kelly, T. Kessler, S. Kumpan, S. Loucks, S. Letzring, F. Marshall, R. McCrory, S. Morse, W. Seka, J. Soures, and C. Verdon, "Initial performance results of the OMEGA laser system," Opt. Commun. **133**, 495–506 (1997).
[21]V. Y. Glebov, C. J. Forrest, K. L. Marshall, M. Romanofsky, T. C. Sangster, M. J. Shoup, and C. Stoeckl, "A new neutron time-of-flight detector for fuel-areal-density measurements on OMEGA," Rev. Sci. Instrum. **85**, 11E102 (2014).
[22]R. A. Lerche, D. W. Phillion, and G. L. Tietbohl, "25 ps neutron detector for measuring ICF-target burn history," Rev. Sci. Instrum. **66**, 933–935 (1995).
[23]C. Stoeckl, R. Boni, F. Ehrne, C. J. Forrest, V. Y. Glebov, J. Katz, D. J. Lonobile, J. Magoon, S. P. Regan, M. J. Shoup, A. Sorce, C. Sorce, T. C. Sangster, and D. Weiner, "Neutron temporal diagnostic for high-yield deuterium-tritium cryogenic implosions on OMEGA," Rev. Sci. Instrum. **87**, 053501 (2016).
[24]H. Sio, J. A. Frenje, J. Katz, C. Stoeckl, D. Weiner, M. Bedzyk, V. Glebov, C. Sorce, M. G. Johnson, H. G. Rinderknecht, A. B. Zylstra, T. C. Sangster, S. P. Regan, T. Kwan, A. Le, A. N. Simakov, W. T. Taitano, L. Chacón, B. Keenan, R. Shah, G. Sutcliffe, and R. D. Petrasso, "A particle x-ray temporal diagnostic (PXTD) for studies of kinetic, multi-ion effects, and ion-electron equilibration rates in inertial confinement fusion plasmas at OMEGA (invited)," Rev. Sci. Instrum. **87**, 11D701 (2016).
[25]C. Stoeckl, V. Y. Glebov, D. D. Meyerhofer, W. Seka, B. Yaakobi, R. P. J. Town, and J. D. Zuegel, "Hard x-ray detectors for OMEGA and NIF," Rev. Sci. Instrum. **72**, 1197–1200 (2001).
[26]C. Stoeckl, W. Theobald, S. P. Regan, and M. H. Romanofsky, "Calibration of a time-resolved hard-x-ray detector using radioactive sources," Rev. Sci. Instrum. **87**, 11E323 (2016).
[27]D. K. Bradley, P. M. Bell, O. L. Landen, J. D. Kilkenny, and J. Oertel, "Development and characterization of a pair of 30–40 ps X-ray framing cameras," Rev. Sci. Instrum. **66**, 716–718 (1995).
[28]W. Seka, D. H. Edgell, J. P. Knauer, J. F. Myatt, A. V. Maximov, R. W. Short, T. C. Sangster, C. Stoeckl, R. E. Bahr, R. S. Craxton, J. A. Delettrez, V. N. Goncharov, I. V. Igumenshchev, and D. Shvarts, "Time-resolved absorption in cryogenic and room-temperature direct-drive implosions," Phys. Plasmas **15**, 056312 (2008).
[29]O. Larroche, H. G. Rinderknecht, and M. J. Rosenberg, "Nuclear yield reduction in inertial confinement fusion exploding-pusher targets explained by fuel-pusher mixing through hybrid kinetic-fluid modeling," Phys. Rev. E **98**, 031201 (2018).
[30]O. Larroche, H. G. Rinderknecht, M. J. Rosenberg, N. M. Hoffman, S. Atzeni, R. D. Petrasso, P. A. Amendt, and F. H. Séguin, "Ion-kinetic simulations of D-^{3}He gas-filled inertial confinement fusion target implosions with moderate to large Knudsen number," Phys. Plasmas **23**, 012701 (2016).
[31]B. L. Henke, J. Y. Uejio, G. F. Stone, C. H. Dittmore, and F. G. Fujiwara, "High-energy x-ray response of photographic films: Models and measurement," J. Opt. Soc. Am. B **3**, 1540–1550 (1986).
[32]K. M. Chandler, S. A. Pikuz, T. A. Shelkovenko, M. D. Mitchell, D. A. Hammer, and J. P. Knauer, "Cross calibration of new x-ray films against direct exposure film from 1 to 8 keV using the X-pinch x-ray source," Rev. Sci. Instrum. **76**, 113111 (2005).
[33]H. G. Rinderknecht, P. A. Amendt, S. C. Wilks, and G. Collins, "Kinetic physics in ICF: Present understanding and future directions," Plasma Phys. Controlled Fusion **60**, 064001 (2018).
[34]L. F. Berzak Hopkins, S. L. Pape, L. Divol, N. B. Meezan, A. J. Mackinnon, D. D. Ho, O. S. Jones, S. Khan, J. L. Milovich, J. S. Ross, P. Amendt, D. Casey, P. M. Celliers, A. Pak, J. L. Peterson, J. Ralph, and J. R. Rygg, "Near-vacuum hohlraums for driving fusion implosions with high density carbon ablators," Phys. Plasmas **22**, 056318 (2015).
[35]D. P. Higginson, P. Amendt, N. Meezan, W. Riedel, H. G. Rinderknecht, S. C. Wilks, and G. Zimmerman, "Hybrid particle-in-cell simulations of laser-driven plasma interpenetration, heating, and entrainment," Phys. Plasmas **26**, 112107 (2019).
[36]O. Larroche, "An extended hydrodynamics model for inertial confinement fusion hohlraums," Eur. Phys. J. D **75**, 297 (2021).